Atom Probe Tomography Analysis of Ag Doping in 2D Layered Material $(PbSe)_5(Bi_2Se_3)_3$

Xiaochen Ren,[1] Arunima K. Singh,[2] Lei Fang,[3,4] Mercouri G. Kanatzidis,[3,4] Francesca Tavazza,[2] Albert V. Davydov[2] and Lincoln J. Lauhon[1]

[1]Department of Materials Science Engineering
[3]Department of Chemistry
Northwestern University, Evanston, Illinois 60208, USA

[2]Materials Science and Engineering Division
National Institute of Standards and Technology, Gaithersburg, Maryland 20899, USA

[4]Materials Science Division
Argonne National Laboratory, 9700 South Cass Avenue, Argonne, Illinois 60439, USA

SEPTEMBER 2016

SUBMITTED TO

Nano Letters

Atom Probe Tomography Analysis of Ag Doping in 2D Layered Material $(PbSe)_5(Bi_2Se_3)_3$

Xiaochen Ren[†], *Arunima K. Singh*[‖], *Lei Fang*[‖,^], *Mercouri G. Kanatzidis*[‖,^], *Francesca Tavazza*[‖], *Albert V. Davydov*[‖], *and Lincoln J. Lauhon**[†]

[†]Department of Materials Science and Engineering, and [‖]Department of Chemistry Northwestern University, Evanston, Illinois 60208, United States

^ Materials Science Division, Argonne National Laboratory, 9700 South Cass Avenue, Argonne, Illinois 60439, United States

[‖]Materials Science and Engineering Division, National Institute of Standards and Technology, Gaithersburg, Maryland 20899, USA

ABSTRACT: Impurity doping in two-dimensional (2D) materials can provide a route to tuning electronic properties, so it is important to be able to determine the distribution of dopant atoms within and between layers. Here we report the tomographic mapping of dopants in layered 2D materials with atomic sensitivity and sub-nanometer spatial resolution using atom probe tomography (APT). APT analysis shows that Ag dopes both Bi_2Se_3 and PbSe layers in $(PbSe)_5(Bi_2Se_3)_3$, and correlations in the position of Ag atoms suggest a pairing across neighboring Bi_2Se_3 and PbSe layers. Density functional theory (DFT) calculations confirm the

favorability of substitutional doping for both Pb and Bi, and provide insights into the observed spatial correlations in dopant locations.

KEYWORDS: atom probe tomography, doping, 2D materials, DFT, materials genome initiative.

Table of Contents figure

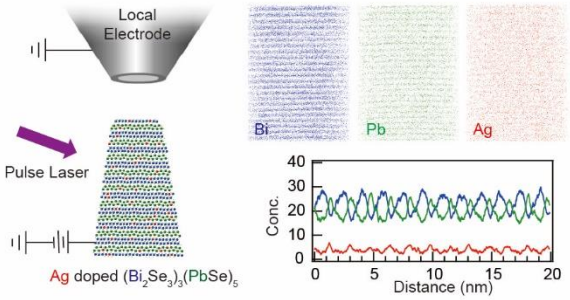

TEXT: Two-dimensional (2D) materials have attracted significant attention due to their unique physical properties[1-3] [4, 5] and potential in device applications [6, 7] [8-10]. Impurity doping plays a central role in controlling the properties of electronic materials, and is beginning to be explored in 2D materials to modulate carrier density[11, 12], engineer the bandgap[13], and impart magnetic properties[14, 15]. One key challenge in doping 2D materials is to measure the dopant distribution, ideally with atomic resolution. Transmission electron microscopy (TEM) and scanning transmission electron microscopy (STEM) have been used to assess the in plane dopant

distribution in 2D materials,[12, 13, 15-17] but atomic resolution in the vertical direction is not routinely achieved. Secondary ion mass spectrometry (SIMS) can reach atomic-scale resolution in depth profiling 2D materials, but its lateral resolution is on the order of 100 nm[18]. Here we report the use of atom probe tomography (APT) and first principles calculations to characterize the atomic scale distribution of Ag dopant atoms in $(PbSe)_5(Bi_2Se_3)_3$, a topological insulator material that can be rendered superconducting by doping with Ag. APT has been used to characterize the three-dimensional dopant distribution in nanowires[19, 20], thin films[21] and FinFET devices[22, 23], but it has not previously been applied to analyze doping in 2D materials. Here, we define 2D materials as materials in which interactions between layers are primarily van der Waals in nature, enabling exfoliation by appropriate techniques. By this definition, $(PbSe)_5(Bi_2Se_3)_3$ can be considered as a 2D material (Supporting information Figure S2).

A significant fraction of the research on 2D materials beyond graphene has focused on transition metal dichalcogenides (TMDs) that can be readily exfoliated and fabricated into conventional electronic devices such as transistors and photodetectors. However, many other layered materials beyond TMDs have intriguing electronic properties that are dramatically impacted by doping. For example, Bi_2Se_3 is a topological insulator[5] whereas Cu doped Bi_2Se_3 is a superconductor.[24] Superconductivity in $Cu_xBi_2Se_3$ is believed to arise from intercalated Cu,[24] but the ratio of intercalated and substitutional Cu atoms is unknown due to experimental limitations in characterizing the atomic scale dopant distribution. $(PbSe)_5(Bi_2Se_3)_{3m}$ is another promising system of homologous materials that consists of *m* layers of Bi_2Se_3 alternating with a layer of PbSe[25]. With an interlayer interaction of van der Waals type this materials can be easily exfoliated into 2D flakes. The *m*=2 phase is a topological insulator[26] that can be made superconducting by Cu doping[27, 28], whereas the semi-metallic *m*=1 phase can be made

superconducting by Ag doping.[29] In this material system, one could in principle create an interface between a superconductor and topological insulator, which has been proposed to host Majorana fermions.[30] Determination of the dopant location is an important step in improving understanding of the material synthesis and properties that could enable fundamentally new types of electronic properties and devices.

Towards this end, APT was used to analyze the location of Ag dopants in Ag doped $(PbSe)_5(Bi_2Se_3)_3$. Despite previous assumptions that Ag atoms would substitute for Pb,[29] Ag is found to dope both Bi_2Se_3 and PbSe layers by APT, and radial distribution functions suggest attractive interactions between Ag atoms. Density functional theory (DFT) calculations of configuration formation energies show that the lowest energy doping configurations involve Ag atoms in each layer. The structural and charge analysis of Ag-doped $(PbSe)_5(Bi_2Se3)_3$ simulated system reveals that the Ag atoms distort the lattice of $(PbSe)_5(Bi_2Se3)_3$ due to lower electropositivity of Ag atoms in comparison to Pb and Bi atoms. The distortion of the lattice is expected to be energetically unfavorable as it is experimentally determined that more than 25 % substitution of Ag in the $(PbSe)_5(Bi_2Se_3)_3$ renders the material unstable[28]. The precise determination of the Ag distribution may inform understanding of the origin of superconductivity in $(PbSe)_5(Bi_2Se_3)_3$ and provide insights as to how to approach the challenge of controlled doping in 2D materials. This work also demonstrates the potential for APT to characterize doping in 2D materials.

The Ag doped $(PbSe)_5(Bi_2Se_3)_3$ was grown by solid state synthesis[29] with a nominal composition of $x \sim 1$ in $Ag_xPb_5Bi_6Se_{14}$, corresponding to a nominal Ag atomic concentration of

0.038. The crystal structure in Figure 1a shows alternately stacked Bi_2Se_3 and PbSe layers, and the weak interlayer bonding is revealed by the fracture surface observed in scanning electron microscopy imaging (Figure 1b). Specimens for APT analysis were prepared using standard focused ion beam (FIB) lift-out and sharpening procedures[31], with the analysis direction perpendicular to (001) planes. The final specimens were sharp needle-shaped tips with diameters less than 100 nm (Figure 1c). APT analysis was performed using a LEAP 4000X Si system* with 355 nm laser of 30 pJ pulse energy and 250 kHz pulse frequency, a 0.005 ions/pulse target detection rate, and a specimen temperature of 28 K. Figure 1d shows a three-dimensional reconstruction of a portion of the specimen (the overall reconstruction can be seen in Figure S1a), mapping Bi atoms as blue dots and Pb atoms as green dots. Alternating layered regions enriched in Bi and Pb layers are visible in the entire reconstruction, and occur with the expected periodicity based on the crystal structure (Fig. 1a).

*Reference to commercial equipment does not imply NIST recommendation or endorsement.

A major motivation for APT doping analysis is the ability to detect single ions with very high spatial resolution. The laser conditions were chosen to optimize the spatial resolution in the analysis direction (Supporting Information Figure S3). The mass spectrum with the chosen laser conditions is shown in Figure 2a. No impurity peaks were detected, and the signal-to-noise level establishes an upper bound of 100 ppm. Peaks for Bi+/Pb+ and Bi++/Pb++ ions can be separated despite the small mass difference between Bi (209 Da) and Pb (204 Da, 206 Da, 207 Da, 208 Da). Peaks for complex ions, such as $BiSe^+$ and $PbSe^+$, $BiSe_2^{++}$ and $PbSe_2^{++}$, overlap due to the large spread of Se isotopes (74 Da to 82 Da). The overlap in peaks in the mass spectrum mixes the assignments of a small fraction of the complex ions, leading to some artificial *spatial* overlap of Bi and Pb elements (Fig. 2b). (Ag is only detected as Ag^+ ions, which do not overlap with other

ions in mass spectrum. Therefore, the 1D concentration profile of Ag does not suffer from spatial overlapping as discussed later). Despite the overlap, alternating Bi_2Se_3 and PbSe layers are resolved in Figure 2b. For a more quantitative statistical analysis of the spatial resolution, we performed a spatial distribution map (SDM) analysis by only counting non-overlapped Bi+/Pb+ and Bi++/Pb++ ions for Bi/Pb. Figure 2c presents the SDM of atoms in the vertical direction of the reconstruction using Bi atoms as the reference species. Briefly, a SDM reports the distribution of one species relative to other atoms of the same or different species. The peak distance in the Bi-Bi profile shows the lattice spacing to be 1.65 nm in the analysis direction, in agreement with the crystal structure. Furthermore, the peaks at ±0.85 nm in the Bi-Pb profile indicate that Bi atoms and Pb atoms are separated statistically from each other, i.e., Bi_2Se_3 layer and PbSe layers are resolved. In support of this interpretation, a similar analysis of $(PbSe)_5(Bi_2Se_3)_6$ is provided in the Supporting Information online (Fig. S4).

However, atomic planes within the Bi_2Se_3 and PbSe layers are not resolved. The imaging of atomic planes requires a well-defined field evaporation sequence in which atoms from the edges of terraces are first to leave the surface.[32, 33] Atomic planes are often observed in metals, but less often in semiconductors due to penetration of electric field.[33] Although $(PbSe)_5(Bi_2Se_3)_3$ is semi-metallic, the weak van der Waals interactions between layers may result in the simultaneous evaporation of many atoms in the same layer, which will hinder the imaging of atomic planes *within* the layers. This assumption is consistent with the experimental observation that the fraction of multiple hits varies non-monotonically from 66% to 71% in steady evaporation. To our knowledge, APT has not been used previously to analyze 2D materials, with the exception of one recent report of impurity analysis in a graphene monolayer,[34] where the imaging of atomic

planes was not achieved. So it remains an open question whether atomic planes can be resolved in APT of 2D materials.

The 1D concentration profile of Ag in Figure 2b shows two peaks in a lattice period, with large peaks in the same positions as the Pb peaks and small peaks in the same positions as the Bi peaks, indicating that Ag atoms are located in both PbSe and Bi_2Se_3 layers. SDM analysis of the Bi-centered Ag distribution (Bi-Ag profile, Figure 2c) shows more clearly that there are peaks at 0 nm and ±0.825 nm. The peaks at ±0.825 nm confirm that Ag atoms reside in the PbSe layers while peak at 0 nm implies that Ag atoms also reside in the Bi_2Se_3 layers. To determine the local concentration of Ag in Bi_2Se_3 and PbSe layers, the one-dimensional composition profile between the two lines in figure 2b was broken up into 10 segments, with the length of each segment equal to the lattice constant. The 10 segments were averaged together to determine the local Ag concentration. The result is shown in Figure 3a. The average atomic concentration of Ag is 3.5 % in the Bi_2Se_3 layer and peaks at 4.5 % in the PbSe layer. The result suggests that 54 % of the Ag atoms are located in the Bi_2Se_3 layers and 46 % are in the PbSe layers, *e.g.*, Ag atoms are distributed nearly equally in the Bi_2Se_3 and PbSe layers. This direct measurement of local concentration is one of the most important capabilities of APT.

To provide further insights into the Ag distribution, first-principles DFT calculations were used to search for energetically favorable configurations of Ag atoms. A substitution of Ag atoms on Pb and Bi sites is expected due to the similarity in the covalent radii and valencies. The nominal concentration of 0.038 can be simulated by substituting 2 Ag atoms in the 50 atom (a = 16.3312

Å, b = 4.2635 Å and c = 21.9245 Å) monoclinic primitive cell of $(PbSe)_5(Bi_2Se_3)_3$ resulting in a 0.040 nominal concentration of Ag. The formation energies, ΔE_{Ag}^{i} , of all configurations with the two Ag atoms restricted to Pb-sites in the PbSe layer (45 configurations), Ag atoms restricted to Bi-sites in the Bi_2Se_3 layer (66 configurations), and Ag atoms distributed equally between Pb-sites and Bi-sites (120 configurations) are computed. A schematic of a configuration with Ag restricted to Pb-sites, Bi-sites and equally distributed in the Pb- and Bi-sites is shown in Figure 3b. ΔE_{Ag}^{i} of the i^{th} configuration is given by,

$$\Delta E_{\mathrm{Ag}}^{i} = E_{\mathrm{Ag}}^{i} - E - n_{\mathrm{Ag}}\mu_{\mathrm{Ag}} + n_{\mathrm{Pb}}\mu_{\mathrm{Pb}} + n_{\mathrm{Bi}}\mu_{\mathrm{Bi}} ,$$

where E_{Ag}^{i} is the energy of the Ag substituted $(PbSe)_5(Bi_2Se_3)_3$ crystal in the i^{th} configuration and E is the energy of the perfect $(PbSe)_5(Bi_2Se_3)_3$ crystal. The number of Ag atoms in the crystal is denoted by n_{Ag} and the number of these Ag atoms on the Pb- and Bi-sites is denoted by n_{Pb} and n_{Bi}, respectively. The phase diagram of PbSe-Bi_2Se_3 system indicates that all the constituent phases are in molten state at the 1223 K synthesis temperature of the crystal,[35] hence the chemical potential of Ag, Pb and Bi atoms, $\mu_{\mathrm{Ag}}, \mu_{\mathrm{Pb}}, \mu_{\mathrm{Bi}}$, respectively, are taken to be the energies of the isolated atoms.

Figure 4a shows the formation energies of the configurations plotted against the distance between the Ag atoms. The distance between the Ag atoms is computed by ignoring the self-images in the periodic images. The formation energies of configurations with Ag atoms equally distributed on the Pb- and Bi-sites are significantly lower than those with Ag atoms restricted to the Pb-sites or Bi-sites only. Figure 4 (b) shows the thermodynamic probability of occurrence of

the i^{th} configuration computed as, $P^i = \frac{e^{\left(\frac{-\Delta E^i_{Ag}}{k_B.T}\right)}}{\sum_{i=1-231} e^{\left(\frac{-\Delta E^i_{Ag}}{k_B.T}\right)}}$, where k_B is the Boltzmann constant and temperature T=300 K. At room temperature, configurations with Ag in both layers account for more than 99.99 % of the total probabilities. Even at temperatures as high as 923 K, configurations with Ag in both layers account for more than 97.57 % of the total probabilities. Thus, the DFT calculations support the experimental observation that Ag dopants are distributed between both Pb and Bi layers.

For the analysis above, all 231 possible configurations were simulated for the *primitive* cell of $(PbSe)_5(Bi_2Se_3)_3$. We note, however, that the Ag-Ag distance in the periodic images in the *y*-direction is restricted to the length of the *y*-lattice vector, *i.e.* 4.26 Å; larger supercells are preferred to avoid artificial interactions between the dopant sites, which in the "real" material do not share the translational symmetry of the lattice.[36] However, a supercell that is 1X2X1 times larger than the primitive cell will not only have larger number of total atoms, but will also require simulating ${}^{44}C_4$ =135751 configurations (4 Ag atoms to be arranged in 44 cation sites). Since simulating all the configurations is beyond the capacity of present-day computational resources, we simulated 9 representative configurations of a 1X2X1 supercell. We find that the configurations where Ag atoms are distributed in both the layers have lower formation energies (See Supporting Information online), consistent with experimental findings.

A structural analysis of all the 240 configurations (See Supporting Information online) reveals that Ag dopants distort the lattice of the crystal and the configurations with lowest formation energies have minimal distortion in the crystal. A Bader charge analysis of the configurations shows that the low energy configurations have localized charge modulation around the Ag dopants. Large distortions in the lattice planes are expected when $(PbSe)_5(Bi_2Se_3)_3$ is doped with a high concentration of Ag. This has been experimentally observed in the form of an instability when $(PbSe)_5(Bi_2Se_3)_3$ is doped with 25 % Ag[28]. Most likely, these distortions are mediated by significantly lower charge of the Ag atoms in comparison to that of Bi and Pb cations (See Supporting Information online for full discussion).

The observation of sharp peaks in the probability distribution of Figure 4(b) raises the question of whether there are correlations in the distribution of Ag atoms within and between layers. In other words, does the presence of a Ag atom influence the probability of finding another Ag atom nearby? To investigate correlations in the Ag distribution, the Ag-Ag radial distribution function (RDF) was generated from the APT data (Fig. 4(c)). A RDF gives the probability of finding an atom B surrounding atom A as a function of distance.[37, 38] The RDF was generated using data from the center of the reconstruction, which has been shown to improve the resolution[38] (SI Figure S5), and is plotted for distances greater than 0.2 nm because ion trajectory effects complicate interpretation at smaller distances.[37] The uncertainty of the measured RDF was evaluated by measuring the standard deviation of 10 simulations with randomly distributed Ag (black curve, Fig 4). The uncertainty is much smaller the deviation of the Ag-Ag RDF from a random distribution. The Ag-Ag RDF shows an increased probability of finding Ag atoms ~7 Å apart, implying a pairwise correlation in Ag dopant distribution. In other words, the average

distance from a given Ag atom to the next closest Ag atom is less than the average distance between Ag atoms. Furthermore, figure S8 shows that the pairing occurs primarily between Ag atoms in adjacent Bi_2Se_3 and PbSe sub-layers by presenting RDF analyses within each sublayer (weakest correlations) and between sublayers (strongest correlations).

To summarize, we have demonstrated that APT can provide new insights into the dopant distribution in 2D materials. APT has the potential to be applied to other 2D materials, such as transition metal dichalcogenides, and can therefore play an important role in the development of controlled doping schemes. First-principles DFT calculations can provide support for an understanding of experimental results, and may be further employed to explain the origin of physical properties based on the dopant distribution confirmed by APT. The combination of APT and first-principles calculations has the potential to significantly advance knowledge of structure property relationships at the atomic and nanoscale.

FIGURES

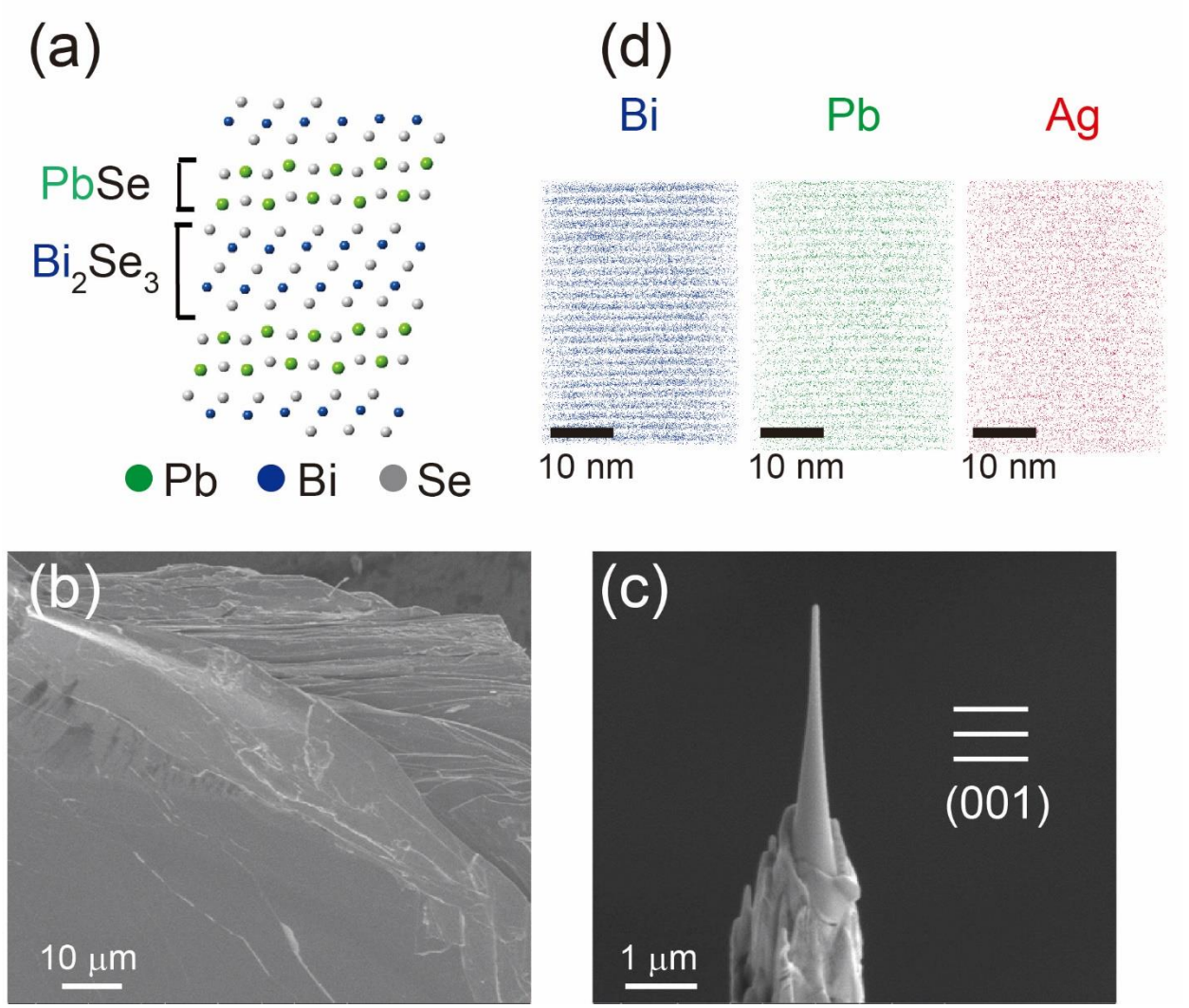

Figure 1. (a) Crystal structure of $(PbSe)_5(Bi_2Se_3)_3$ with alternating PbSe and Bi_2Se_3 layers. (b) Top view SEM image of the $(PbSe)_5(Bi_2Se_3)_3$ crystal. (c) SEM image of a sharpened tip. (d) A region of interest in the reconstruction with the distribution of Bi, Pb and Ag, showing that layers are resolved.

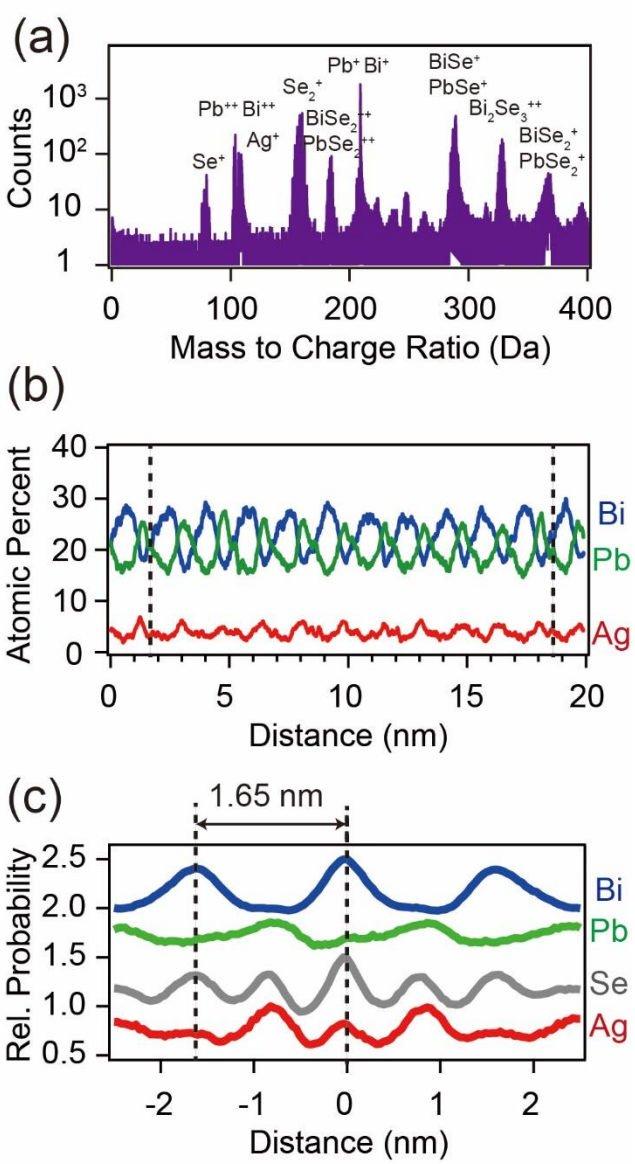

Figure 2. (a) Mass spectrum taken at 30 pJ laser pulse energy. (b) 1D concentration profiles in the region of interest shown in Figure 1d. (c) SDM of atoms relative to Bi atoms (curves are offset by 0.5 units each for clarity).

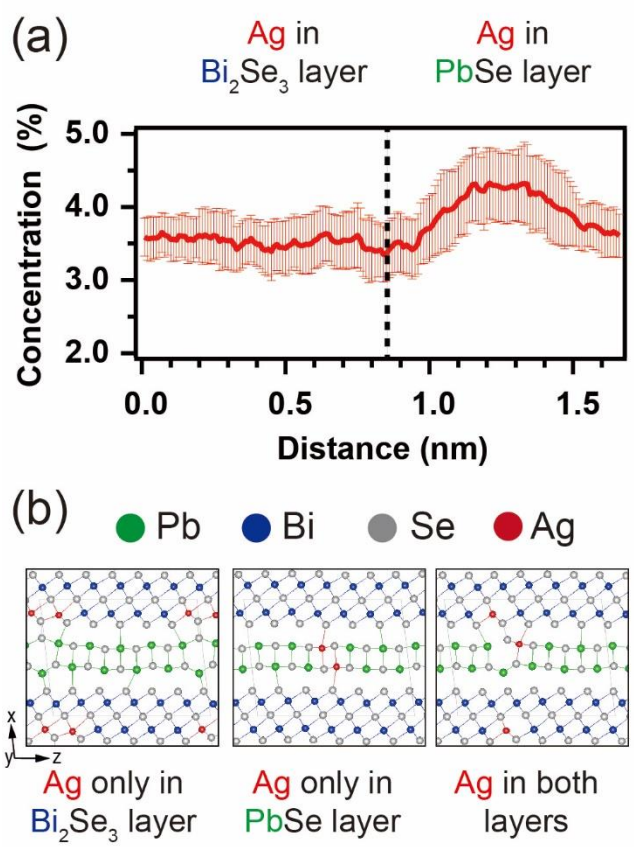

Figure 3. (a) 1D concentration profile of Ag obtained by averaging the data shown in Figure 2b over 10 unit cells. (b) Schematics of example configurations of Ag dopant atoms with Ag restricted to Pb sites, Bi sites, and equally distributed between Pb and Bi sites, respectively. The *y* direction is normal to the plane of the figure.

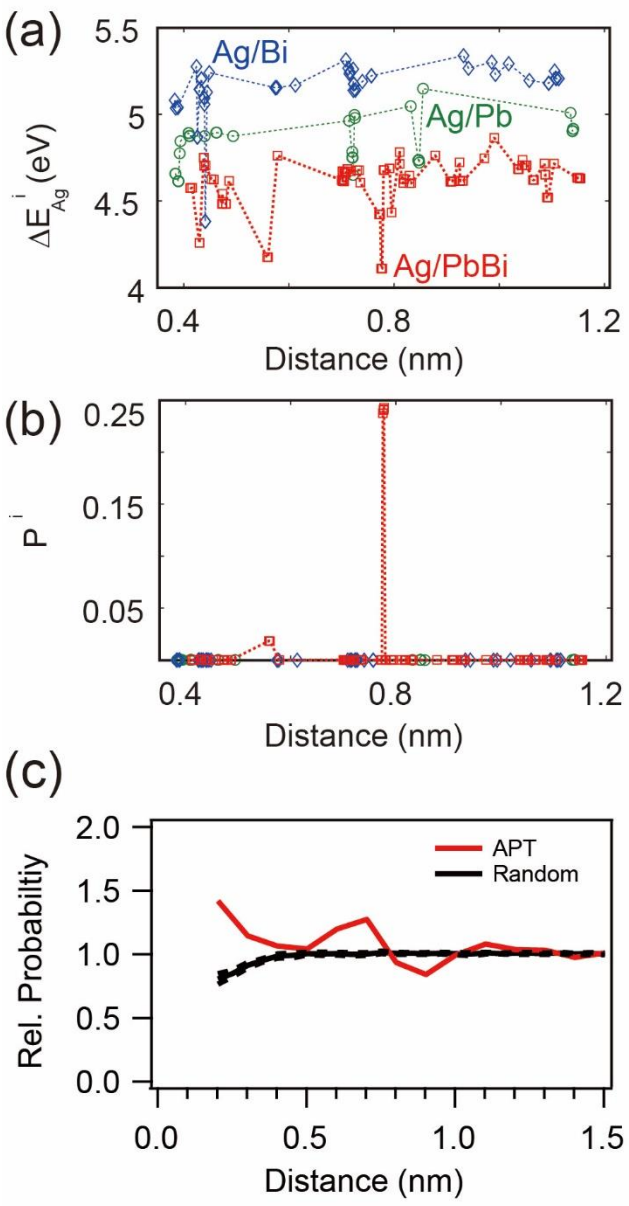

Figure 4. (a) Defect Formation energies of different configurations of Ag dopants plotted against distance between pairs of Ag atoms. (b) Probabilities of occurance of Ag-Ag configurations at 300 K. (c) Ag-Ag radial distribution function from APT reconstruction compared with that of randomly distributed Ag atoms.

ASSOCIATED CONTENT

Supporting Information. Methods, calculation of interlayer bonding strength of $(PbSe)_5(Bi_2Se_3)_3$, influence of laser energy on $(PbSe)_5(Bi_2Se_3)_3$, APT analysis of $(PbSe)_5(Bi_2Se_3)_6$, structural and charge analysis of configurations contributing to 99.99 % of total probabilities at 300 K, formation energies of representative 1X2X1 supercell configurations and analysis of Ag pairing. This material is available free of charge via the Internet at http://pubs.acs.org.

AUTHOR INFORMATION

Corresponding Author

*E-mail: lauhon@northwestern.edu.

Notes

The authors declare no competing financial interest.

ACKNOWLEDGMENT

This work was supported by Center for Hierarchical Materials Design (U.S. Department of Commerce, NIST 70NANB14H012). F. Tavazza and A. Davydov are funded by the Materials Genome Initiative funding allocated to National Institute of Standards and Technology (NIST). A. Singh is funded by the Professional Research Experience Postdoctoral Fellowship under

Award No. 70NANB11H012. Atom-probe tomography was performed at the Northwestern University Center for Atom-Probe Tomography (NUCAPT), which is a Shared Facility at the Materials Research Center of Northwestern University, supported by the National Science Foundation's MRSEC program (DMR-1121262). Work at Argonne National Laboratory was supported by the U.S. Department of Energy, Office of Science, Materials Sciences and Engineering Division. Computational resources were provided by the Texas Advanced Computing Center under Contract No. TG-DMR150006. This work used the Extreme Science and Engineering Discovery Environment (XSEDE), which is supported by the National Science Foundation Grant No. ACI-1053575. The authors thank R. G. Hennig for helpful discussions.

ABBREVIATIONS

2D, two-dimensional; SEM, scanning electron microscopy; TEM, transmission electron microscopy; STEM, scanning transmission electron microscopy; SIMS, secondary ion mass spectrometry; APT, atom probe tomography; TMDs, transition metal dichalcogenides; DFT, density functional theory; FIB, focused ion beam; SDM, spatial distribution map; RDF, radial distribution function.

REFERENCES:

1. Castro Neto, A. H.; Guinea, F.; Peres, N. M. R.; Novoselov, K. S.; Geim, A. K. The Electronic Properties of Graphene. *Rev. Mod. Phys.* **2009**,81, 109-162.
2. Wang, Q. H.; Kalantar-Zadeh, K.; Kis, A.; Coleman, J. N.; Strano, M. S. Electronics and Optoelectronics of Two-Dimensional Transition Metal Dichalcogenides. *Nat. Nanotechnol.* **2012**,7, 699-712.
3. Butler, S. Z.; Hollen, S. M.; Cao, L. Y.; Cui, Y.; Gupta, J. A.; Gutierrez, H. R.; Heinz, T. F.; Hong, S. S.; Huang, J. X.; Ismach, A. F.; Johnston-Halperin, E.; Kuno, M.; Plashnitsa, V. V.;

Robinson, R. D.; Ruoff, R. S.; Salahuddin, S.; Shan, J.; Shi, L.; Spencer, M. G.; Terrones, M.; Windl, W.; Goldberger, J. E. Progress, Challenges, and Opportunities in Two-Dimensional Materials Beyond Graphene. *ACS Nano* **2013**,7, 2898-2926.
4. Xia, Y.; Qian, D.; Hsieh, D.; Wray, L.; Pal, A.; Lin, H.; Bansil, A.; Grauer, D.; Hor, Y. S.; Cava, R. J.; Hasan, M. Z. Observation of a Large-Gap Topological-Insulator Class with a Single Dirac Cone on the Surface. *Nat. Phys.* **2009**,5, 398-402.
5. Zhang, H. J.; Liu, C. X.; Qi, X. L.; Dai, X.; Fang, Z.; Zhang, S. C. Topological Insulators in Bi_2Se_3, Bi_2Te_3 and Sb_2Te_3 with a Single Dirac Cone on the Surface. *Nat. Phys.* **2009**,5, 438-442.
6. Radisavljevic, B.; Radenovic, A.; Brivio, J.; Giacometti, V.; Kis, A. Single-Layer MoS_2 Transistors. *Nat. Nanotechnol.* **2011**,6, 147-150.
7. Rycerz, A.; Tworzydlo, J.; Beenakker, C. W. J. Valley Filter and Valley Valve in Graphene. *Nat. Phys.* **2007**,3, 172-175.
8. Schedin, F.; Geim, A. K.; Morozov, S. V.; Hill, E. W.; Blake, P.; Katsnelson, M. I.; Novoselov, K. S. Detection of Individual Gas Molecules Adsorbed on Graphene. *Nat. Mater.* **2007**,6, 652-655.
9. Yin, Z. Y.; Li, H.; Li, H.; Jiang, L.; Shi, Y. M.; Sun, Y. H.; Lu, G.; Zhang, Q.; Chen, X. D.; Zhang, H. Single-Layer MoS_2 Phototransistors. *ACS Nano* **2012**,6, 74-80.
10. Withers, F.; Del Pozo-Zamudio, O.; Mishchenko, A.; Rooney, A. P.; Gholinia, A.; Watanabe, K.; Taniguchi, T.; Haigh, S. J.; Geim, A. K.; Tartakovskii, A. I.; Novoselov, K. S. Light-emitting diodes by band-structure engineering in van der Waals heterostructures. *Nat. Mater.* **2015**,14, 301-306.
11. Fang, H.; Tosun, M.; Seol, G.; Chang, T. C.; Takei, K.; Guo, J.; Javey, A. Degenerate n-Doping of Few-Layer Transition Metal Dichalcogenides by Potassium. *Nano Lett.* **2013**,13, 1991-1995.
12. Suh, J.; Park, T.-E.; Lin, D.-Y.; Fu, D.; Park, J.; Jung, H. J.; Chen, Y.; Ko, C.; Jang, C.; Sun, Y.; Sinclair, R.; Chang, J.; Tongay, S.; Wu, J. Doping against the Native Propensity of MoS2: Degenerate Hole Doping by Cation Substitution. *Nano lett.* **2014**,14, 6976-6982.
13. Gong, Y. J.; Liu, Z.; Lupini, A. R.; Shi, G.; Lin, J. H.; Najmaei, S.; Lin, Z.; Elias, A. L.; Berkdemir, A.; You, G.; Terrones, H.; Terrones, M.; Vajtai, R.; Pantelides, S. T.; Pennycook, S. J.; Lou, J.; Zhou, W.; Ajayan, P. M. Band Gap Engineering and Layer-by-Layer Mapping of Selenium-Doped Molybdenum Disulfide. *Nano Lett.* **2014**,14, 442-449.
14. Cheng, Y. C.; Zhu, Z. Y.; Mi, W. B.; Guo, Z. B.; Schwingenschlogl, U. Prediction of Two-Dimensional Diluted Magnetic Semiconductors: Doped Monolayer MoS_2 Systems. *Phys. Rev. B* **2013**,87, 100401.
15. Zhang, K.; Feng, S.; Wang, J.; Azcatl, A.; Lu, N.; Addou, R.; Wang, N.; Zhou, C.; Lerach, J.; Bojan, V.; Kim, M. J.; Chen, L.-Q.; Wallace, R. M.; Terrones, M.; Zhu, J.; Robinson, J. A. Manganese Doping of Monolayer MoS_2: The Substrate Is Critical. *Nano Lett.* **2015**,15, 6586-6591.
16. Laskar, M. R.; Nath, D. N.; Ma, L.; Lee, E. W.; Lee, C. H.; Kent, T.; Yang, Z.; Mishra, R.; Roldan, M. A.; Idrobo, J.-C.; Pantelides, S. T.; Pennycook, S. J.; Myers, R. C.; Wu, Y.; Rajan, S. P-type Doping of MoS_2 Thin Films Using Nb. *App. Phys. Lett.* **2014**,104, 092104.
17. Lin, Y.-C.; Dumcenco, D. O.; Komsa, H.-P.; Niimi, Y.; Krasheninnikov, A. V.; Huang, Y.-S.; Suenaga, K. Properties of Individual Dopant Atoms in Single-Layer MoS_2 : Atomic Structure, Migration, and Enhanced Reactivity. *Adv. Mater.* **2014**,26, 2857-2861.

18. Chou, H.; Ismach, A.; Ghosh, R.; Ruoff, R. S.; Dolocan, A. Revealing the planar chemistry of two-dimensional heterostructures at the atomic level. *Nature Communications* **2015**,6.
19. Perea, D. E.; Hemesath, E. R.; Schwalbach, E. J.; Lensch-Falk, J. L.; Voorhees, P. W.; Lauhon, L. J. Direct Measurement of Dopant Distribution in an Individual Vapour-Liquid-Solid Nanowire. *Nat. Nanotechnol.* **2009**,4, 315-319.
20. Moutanabbir, O.; Isheim, D.; Blumtritt, H.; Senz, S.; Pippel, E.; Seidman, D. N. Colossal Injection of Catalyst Atoms into Silicon Nanowires. *Nature* **2013**,496, 78-82.
21. Cojocaru-Miredin, O.; Choi, P.; Wuerz, R.; Raabe, D. Atomic-Scale Characterization of the CdS/$CuInSe_2$ Interface in Thin-Film Solar Cells. *Appl. Phys. Lett.* **2011**,98, 103504.
22. Kambham, A. K.; Mody, J.; Gilbert, M.; Koelling, S.; Vandervorst, W. Atom-Probe for FinFET Dopant Characterization. *Ultramicroscopy* **2011**,111, 535-539.
23. Kambham, A. K.; Kumar, A.; Florakis, A.; Vandervorst, W. Three-Dimensional Doping and Diffusion in Nano Scaled Devices as Studied by Atom Probe Tomography. *Nanotechnology* **2013**,24, 275705.
24. Hor, Y. S.; Williams, A. J.; Checkelsky, J. G.; Roushan, P.; Seo, J.; Xu, Q.; Zandbergen, H. W.; Yazdani, A.; Ong, N. P.; Cava, R. J. Superconductivity in $Cu_xBi_2Se_3$ and its Implications for Pairing in the Undoped Topological Insulator. *Phys. Rev. Lett.* **2010**,104, 057001.
25. Kanatzidis, M. G. Structural Evolution and Phase Homologies for "Design" and Prediction of Solid-State Compounds. *Acc. Chem. Res.* **2005**,38, 359-368.
26. Nakayama, K.; Eto, K.; Tanaka, Y.; Sato, T.; Souma, S.; Takahashi, T.; Segawa, K.; Ando, Y. Manipulation of Topological States and the Bulk Band Gap Using Natural Heterostructures of a Topological Insulator. *Phys. Rev. Lett.* **2012**,109, 236804.
27. Sasaki, S.; Segawa, K.; Ando, Y. Superconductor Derived from a Topological Insulator Heterostructure. *Phys. Rev. B* **2014**,90, 220504.
28. Nakayama, K.; Kimizuka, H.; Tanaka, Y.; Sato, T.; Souma, S.; Takahashi, T.; Sasaki, S.; Segawa, K.; Ando, Y. Observation of Two-Dimensional Bulk Electronic States in the Superconducting Topological Insulator Heterostructure $Cu_x(PbSe)_5(Bi2Se3)_6$: Implications for Unconventional Superconductivity. *Phys. Rev. B* **2015**,92, 100508.
29. Fang, L.; Stoumpos, C. C.; Jia, Y.; Glatz, A.; Chung, D. Y.; Claus, H.; Welp, U.; Kwok, W. K.; Kanatzidis, M. G. Dirac Fermions and Superconductivity in the Homologous Structures $(Ag_xPb_{1-x}Se)_5(Bi2Se3)_{3m}$ (m=1,2). *Phys. Rev. B* **2014**,90, 020504.
30. Fu, L.; Kane, C. L. Superconducting Proximity Dffect and Majorana Fermions at the Surface of a Topological Insulator. *Phys. Rev. Lett.* **2008**,100, 096407.
31. Thompson, K.; Lawrence, D.; Larson, D. J.; Olson, J. D.; Kelly, T. F.; Gorman, B. In situ Site-Specific Specimen Preparation for Atom Probe Tomography. *Ultramicroscopy* **2007**,107, 131-139.
32. Gruber, M.; Vurpillot, F.; Bostel, A.; Deconihout, B. Field Evaporation: A Kinetic Monte Carlo Approach on the Influence of Temperature. *Surf. Sci.* **2011**,605, 2025-2031.
33. Gault, B.; Moody, M. P.; Cairney, J. M.; Ringer, S. P. Atom Probe Crystallography. *Mater. Today* **2012**,15, 378-386.
34. Baik, S.-I.; Ma, L.; Kim, Y.-J.; Li, B.; Liu, M.; Isheim, D.; Yakobson, B. I.; Ajayan, P. M.; Seidman, D. N. An Atomistic Tomographic Study of Oxygen and Hydrogen Atoms and their Molecules in CVD Grown Graphene. *Small* **2015**,11, 5968-5974.
35. Shelimova, L. E.; Karpinskii, O. G.; Zemskov, V. S. X-Ray Diffraction Study of Ternary Layered Compounds in the PbSe-Bi_2Se_3 System. *Inorg. Mater.* **2008**,44, 927-931.

36. Freysoldt, C.; Grabowski, B.; Hickel, T.; Neugebauer, J.; Kresse, G.; Janotti, A.; Van de Walle, C. G. First-principles calculations for point defects in solids. *Rev. Mod. Phys.* **2014**,86, 253.
37. Sudbrack, C. K.; Noebe, R. D.; Seidman, D. N. Direct Observations of Nucleation in a Nondilute Multicomponent Alloy. *Phys. Rev. B* **2006**,73, 212101.
38. Haley, D.; Petersen, T.; Barton, G.; Ringer, S. P. Influence of Field Evaporation on Radial Distribution Functions in Atom Probe Tomography. *Philos. Mag.* **2009**,89, 925-943.